

# Neural Progenitor Cells Alter Chromatin Organization and Neurotrophin Expression in Response to 3D Matrix Degradability

Christopher M. Madl, Bauer L. LeSavage, Margarita Khariton, and Sarah C. Heilshorn\*

Neural progenitor cells (NPCs) are promising therapeutic candidates for nervous system regeneration. Significant efforts focus on developing hydrogel-based approaches to facilitate the clinical translation of NPCs, from scalable platforms for stem cell production to injectable carriers for cell transplantation. However, fundamental questions surrounding NPC-hydrogel interactions remain unanswered. While matrix degradability is known to regulate the stemness and differentiation capacity of NPCs, how degradability impacts NPC epigenetic regulation and secretory phenotype remains unknown. To address this question, NPCs encapsulated in recombinant protein hydrogels with tunable degradability are assayed for changes in chromatin organization and neurotrophin expression. In high degradability gels, NPCs maintain expression of stem cell factors, proliferate, and have large nuclei with elevated levels of the stemness-associated activating histone mark H3K4me3. In contrast, NPCs in low degradability gels exhibit more compact, rounded nuclei with peripherally localized heterochromatin, are non-proliferative yet non-senescent, and maintain expression of neurotrophic factors with potential therapeutic relevance. This work suggests that tuning matrix degradability may be useful to direct NPCs toward either a more-proliferative, stem-like phenotype for cell replacement therapies, or a more quiescent-like, pro-secretory phenotype for soluble factor-mediated therapies.

neural function.<sup>[1]</sup> NPCs are capable of differentiation into the major cell types of the central nervous system: neurons, astrocytes, and oligodendrocytes.<sup>[1]</sup> As such, NPC transplantation has been extensively studied as a means for replacing damaged nervous tissue.<sup>[2]</sup> NPCs also secrete numerous neurotrophic and immune modulatory factors and have thus been suggested as potential “living drug depots” to influence the healing response, guiding reinnervation, and limiting scarring.<sup>[3]</sup>

Despite their therapeutic promise, NPCs have yet to achieve widespread use in clinical practice.<sup>[4]</sup> Translation of NPC therapies is limited by the same bottlenecks that hamper other stem cell therapies, including difficulty expanding high quality NPCs in a robust and cost-effective manner, significant cell loss during transplantation, and limited ability to control the fate of transplanted cells.<sup>[5,6]</sup> To overcome these limitations, a variety of materials-based approaches are being developed to expand stem cells, protect cells during transplantation, and direct cell fate in vivo.<sup>[6]</sup> Hydrogels are an attractive class of materials for cell culture and transplantation, as their physical

## 1. Introduction

The transplantation of neural progenitor cells (NPCs) to sites of central nervous system injury is a promising approach to restore


and biochemical properties can be tuned to recapitulate key aspects of the native cellular microenvironment.<sup>[7]</sup> Accordingly, a variety of approaches utilizing hydrogels have been investigated for cell therapies to promote neural regeneration.<sup>[8]</sup> Nevertheless, many fundamental questions regarding how NPCs are influenced by hydrogel biomaterials remain and must be addressed before materials-based strategies can move forward to the clinic.

We recently reported that encapsulated NPCs must be able to degrade or remodel the surrounding hydrogel matrix to maintain their stem cell phenotype and subsequently differentiate into mature cell types (**Figure 1A**).<sup>[9,10]</sup> While demonstrating that matrix degradability was a crucial regulator of NPC stemness and differentiation capacity, our previous studies did not address two key questions for future therapeutic use of hydrogel-embedded NPCs: 1) How does matrix remodeling alter the epigenetic state of NPCs, and 2) how does matrix remodeling regulate the secretory phenotype of NPCs? In the present study, we leverage our recombinant protein hydrogel system with quantitative tuning of matrix degradability to determine how degradability alters NPC chromatin organization and neurotrophin expression. Our results suggest that hydrogel degradability can tune the

Dr. C. M. Madl, Dr. B. L. LeSavage, Dr. M. Khariton  
Department of Bioengineering  
Stanford University  
Stanford, CA 94305, USA

Dr. C. M. Madl  
Baxter Laboratory for Stem Cell Biology  
Department of Microbiology & Immunology  
Stanford University  
Stanford CA 94305, USA

Prof. S. C. Heilshorn  
Department of Materials Science & Engineering  
Stanford University  
476 Lomita Mall, McCullough Room 246 Stanford, CA 94305, USA  
E-mail: heilshorn@stanford.edu

 The ORCID identification number(s) for the author(s) of this article can be found under <https://doi.org/10.1002/adhm.202000754>

DOI: 10.1002/adhm.202000754

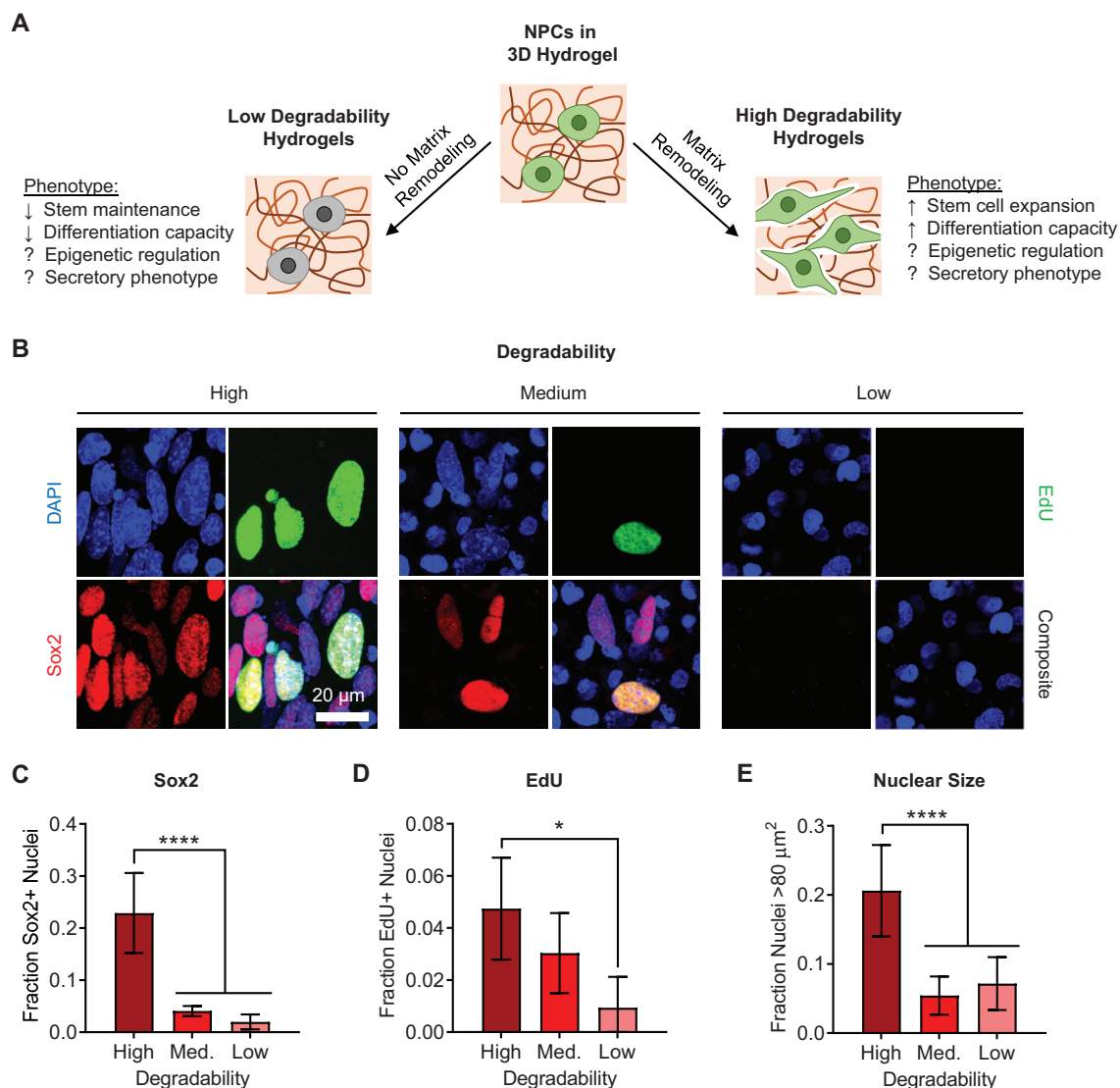


**Figure 1.** Matrix degradability regulates NPC transcriptional activity, proliferation, and nuclear morphology. A) Schematic depicting ways in which matrix remodeling can impact NPC phenotype, highlighting that epigenetic changes and alterations in secretory phenotype remain unexplored. B) Immunofluorescence imaging of nuclei for NPCs cultured for 7 days in ELP hydrogels with varying degradability. Blue: DAPI (DNA); green: EdU; red: Sox2. NPCs cultured in high degradability gels exhibit increased fractions of nuclei that are positive for C) the stemness-associated transcription factor Sox2 and D) EdU incorporation and E) that are relatively large in size (projected nuclear area >80  $\mu\text{m}^2$ ). Data are presented as mean  $\pm$  s.d.  $n = 8$  independent gels for Sox2 and nuclear size and 4 independent gels for EdU. \* $p < 0.05$ , \*\*\*\* $p < 0.0001$ , one-way ANOVA with Bonferroni post hoc test.

phenotype of encapsulated NPCs to behave either like activated progenitor cells that can differentiate and replace damaged tissue or like non-proliferative cells that can secrete paracrine factors to indirectly modulate regeneration.

## 2. Results

### 2.1. Nuclear Morphology Is Correlated with NPC Stemness and Proliferation

To assess how matrix remodeling alters NPC phenotype, adult murine NPCs isolated from microdissected dentate gyrus were encapsulated within hydrogels comprised of recombinantly

expressed engineered elastin-like proteins (ELPs). The ELPs consist of repeating modular domains that contain either bioactive cues, including cell-adhesive ligands and proteolytic degradation sites, or structural components, namely the elastin-like amino acid sequence VPGXG, wherein one out of five X residues is a lysine used to crosslink the proteins into hydrogel networks (Figure S1A,B, Supporting Information).<sup>[11]</sup> By varying the stoichiometry of lysines relative to the small molecule cross-linker tetrakis(hydroxymethyl)phosphonium chloride (THPC) at a constant polymer mass fraction, we have previously demonstrated that we can tune the bulk degradability of the ELP hydrogels while maintaining a matrix stiffness ( $E \approx 0.5\text{--}1.5$  kPa) appropriate for the culture of NPCs (Figure S1C, Supporting Information).<sup>[9,10]</sup> The ELPs used in this study contain an integrin-binding

arginine-glycine-aspartic acid (RGD) sequence to enable specific cell–matrix adhesion, as well as a peptide sequence susceptible to proteolytic cleavage by the NPC-produced protease, a disintegrin, and metalloprotease 9 (ADAM9), to enable cell-mediated degradation of the hydrogel network (Figure S1B, Supporting Information).

NPCs were encapsulated within THPC-crosslinked ELP hydrogels with high, medium, or low degradability and cultured for 7 days in medium that promotes stem cell maintenance. To determine how hydrogel degradability impacts the stem properties of NPCs, the cells were first treated with the thymidine analogue EdU on day 6 to mark proliferative cells. The cells were then fixed on day 7 and immunostained for protein markers characteristic of multipotent neural progenitors (Figure 1B). The fraction of cells staining positive for the stem cell transcription factor Sox2 was highest in the high degradability gels and decreased with decreasing degradability (Figure 1C). The same trend was observed for EdU incorporation (Figure 1D), indicating that cells were most proliferative in the high degradability gels. Increased proliferation in high degradability gels was further validated by comparing nuclear counts and DNA content in hydrogels with tunable degradability (Figure S2, Supporting Information). Furthermore, cells that stained positive for Sox2 and EdU co-stain for the neural stemness marker nestin (Figure S3, Supporting Information). These findings are consistent with our previous results, which indicated that matrix remodeling was necessary for NPCs to maintain their stem cell phenotype.<sup>[9]</sup>

Intriguingly, significant changes in nuclear morphology were also observed as hydrogel degradability was altered. A greater fraction of NPCs in high degradability hydrogels had large nuclei, defined as nuclei with projected area  $>80 \mu\text{m}^2$  (Figure 1E). To further investigate whether maintenance of stemness was correlated with changes in nuclear morphology, we analyzed the size and shape of nuclei that were positive versus negative for Sox2 or EdU across all hydrogel degradabilities tested (Figure 2). A striking distinction was observed between the two groups of nuclei: those positive for Sox2 or EdU (and thus more stem-like) were significantly larger in projected area (Figure 2B,D,G,I; Figures S4 and S6, Supporting Information) and were significantly less round (Figure 2C,E,H,J; Figures S5 and S7, Supporting Information), adopting a more oblong morphology (Figure 2A,F). This trend was consistent for NPCs cultured in all three degradability conditions. While the fraction of nuclei positive for Sox2 and EdU decreases with decreasing degradability (Figure 1B–D), within each degradability condition, those nuclei that are positive for Sox2 and EdU are significantly larger and less round (Figure 2B,C,G,H).

## 2.2. Matrix Remodeling Promotes Activating Histone Modification

Because of the marked differences observed in nuclear morphology between cells that were positive versus negative for Sox2 and EdU, we hypothesized that chromatin organization would vary with hydrogel degradability. We first considered canonical activating epigenetic modifications, specifically trimethylation at lysine 4 of histone 3 (H3K4me3),<sup>[12]</sup> which has been shown to be correlated with expression of neural stem markers in primate

subventricular zone.<sup>[13]</sup> NPCs cultured in high, medium, or low degradability gels were fixed after 7 days in maintenance medium and immunostained for Sox2 and H3K4me3 (Figure 3A). As expected, the intensity of nuclear Sox2 staining decreased with decreasing degradability (Figure 3B). H3K4me3 staining exhibited the same trend, with significantly lower H3K4me3 intensity observed in medium and low degradability gels compared to high degradability gels (Figure 3C). To determine if H3K4me3 staining was associated with stemness maintenance, we performed correlation analyses of Sox2 and H3K4me3 intensities for each nuclear region of interest assayed. Across all three degradability conditions, Sox2 and H3K4me3 intensities were positively correlated (Figure 3D). Within the individual degradability conditions, high correlation was observed for high and medium degradability samples (Spearman coefficients of  $\approx 0.90$  and  $\approx 0.84$ , respectively), which contain significant populations of cells with strong staining for Sox2 and H3K4me3 (Figure S8, Supporting Information). A weaker but statistically significant correlation was observed in low degradability gels that had very few cells strongly staining for Sox2 and H3K4me3 (Figure S8, Supporting Information). Thus, NPCs in higher degradability gels were more likely to exhibit higher levels of the activating chromatin mark H3K4me3, and the increase in this mark was correlated with NPC stemness.

## 2.3. Heterochromatin Organization Varies with Matrix Degradability

We next sought to investigate whether changes in nuclear morphology and NPC stemness arising from altered hydrogel degradability impact the organization of transcriptionally inactive heterochromatin. NPCs cultured in high, medium, or low degradability hydrogels were fixed after 7 days in maintenance medium and immunostained for trimethylation at lysine 9 of histone 3 (H3K9me3), a well-established epigenetic mark associated with heterochromatin (Figure 4A).<sup>[14]</sup> A marked difference in heterochromatin organization was observed in high degradability versus medium and low degradability gels. In the large nuclei common in high degradability gels, dense regions of heterochromatin were distributed throughout the nuclei. In contrast, the smaller, rounded nuclei that predominate in low degradability gels exhibited peripherally localized heterochromatin along the nuclear envelope. High degradability gels had a significantly lower fraction of nuclei with peripheral heterochromatin compared to medium and low degradability gels (Figure 4B). Thus, the organization of heterochromatin within nuclei varied with matrix degradability.

## 2.4. Nuclear Lamina Composition Varies with Matrix Degradability

Due to the significant changes in nuclear morphology and heterochromatin organization observed between NPCs cultured in high versus low degradability hydrogels, we investigated changes in the composition of nuclear structural proteins as a function of hydrogel degradability. Lamins are intermediate filament proteins that assemble into a meshwork along the inner surface of the nuclear envelope.<sup>[15,16]</sup> There are two main classes of

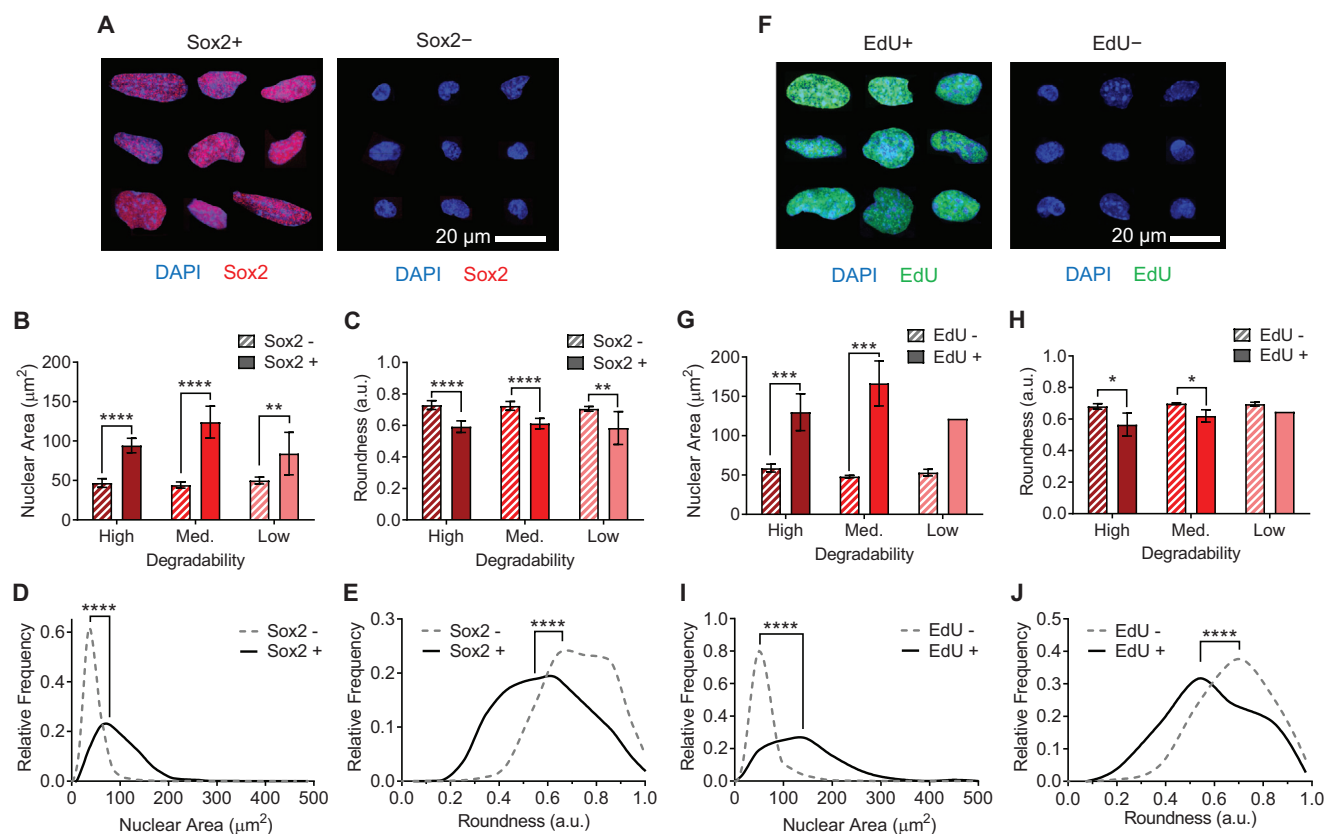


**Figure 2.** Nuclear morphology is correlated with Sox2 expression and EdU incorporation. A) Representative immunofluorescence images of nuclei that are either positive or negative for Sox2 expression, compiled from gels with high, medium, and low degradability. Blue: DAPI (DNA); red: Sox2. Across high, medium, and low degradability gels, nuclei staining positive for Sox2 have B) larger nuclei as measured by projected nuclear area and C) lower nuclear roundness. D,E) Histograms of aggregated nuclei across all conditions showing distribution of nuclear area and roundness for Sox<sup>-</sup> and Sox<sup>+</sup> nuclei. F) Representative immunofluorescence images of nuclei that are either positive or negative for EdU incorporation, compiled from gels with high, medium, and low degradability. Blue: DAPI (DNA); green: EdU. The same trend is observed for EdU incorporation as for Sox2 positivity, with EdU<sup>+</sup> nuclei both G) larger and H) less round than EdU<sup>-</sup> nuclei. I,J) Histograms of aggregated nuclei across all conditions showing distribution of nuclear area and roundness for EdU<sup>-</sup> and EdU<sup>+</sup> nuclei. In (B), (C), (G), and (H), data are presented as mean  $\pm$  s.d.  $n = 8$  independent gels for Sox2 and 4 independent gels for EdU. Only two out of four low degradability gels had any EdU<sup>+</sup> cells, so error bars and statistics are not presented for this comparison. \* $p < 0.05$ , \*\* $p < 0.01$ , \*\*\* $p < 0.001$ , \*\*\*\* $p < 0.0001$ , two-tailed Student's  $t$ -test with Holm-Sidak multiple comparisons correction. In (D), (E), (I), and (J), \*\*\*\* $p < 0.0001$ , Kolmogorov–Smirnov test. Histograms include 1226 Sox<sup>+</sup> nuclei and 9068 Sox<sup>-</sup> nuclei from 24 independent gels (8 of each degradability) and 147 EdU<sup>+</sup> nuclei and 4252 EdU<sup>-</sup> nuclei from 12 independent gels (4 of each degradability). Representative histograms showing nuclear area and roundness for individual replicates are presented in Figures S4–S7, Supporting Information.

lamins expressed in mammalian cells, A-type lamins, consisting of splice variants of the *LMNA* gene (predominantly lamin A and lamin C), and B-type lamins (lamin B1 and lamin B2).<sup>[15,17]</sup> Both classes of lamins contribute to the mechanical properties of nuclei and to chromatin organization.<sup>[15]</sup>

To determine the lamin composition in NPCs cultured in hydrogels of varying degradability, cells were cultured for 7 days in maintenance medium, the gels were mechanically disrupted, and protein lysates were collected for Western blot analysis. Blots were probed for lamin A/C and lamin B1 (Figure 5A). Lamin B1 expression was consistent across samples with different degradability (Figure 5B; Figure S9, Supporting Information), which agrees with prior work demonstrating conserved expression of B-type lamins across various tissues and cell lines.<sup>[18]</sup> In contrast, expression of A-type lamins decreased with decreasing degradability, as the ratio of lamins A/C:B is significantly higher in high degradability gels compared to low degradability gels (Figure 5C).

Interestingly, high degradability gels appear to express a higher ratio of the lamin A splice variant compared to the lamin C splice variant than low degradability gels (Figure 5A). Taken together, these results indicate that the composition of the nuclear lamina varied as a function of hydrogel degradability.

## 2.5. NPCs in Low Degradability Gels Maintain a Pro-Secretory, Non-Senescent Phenotype

The phenotype of NPCs cultured in high degradability gels is consistent with our previous studies reporting an increase in NPC stemness with an increase in matrix remodeling.<sup>[9,10]</sup> In high degradability gels, NPCs express higher levels of stemness markers (Figure 1B,C; Figure 3A,B; Figure S3, Supporting Information), proliferate more (Figure 1B,D; Figures S2 and S3, Supporting Information), and exhibit activating chromatin



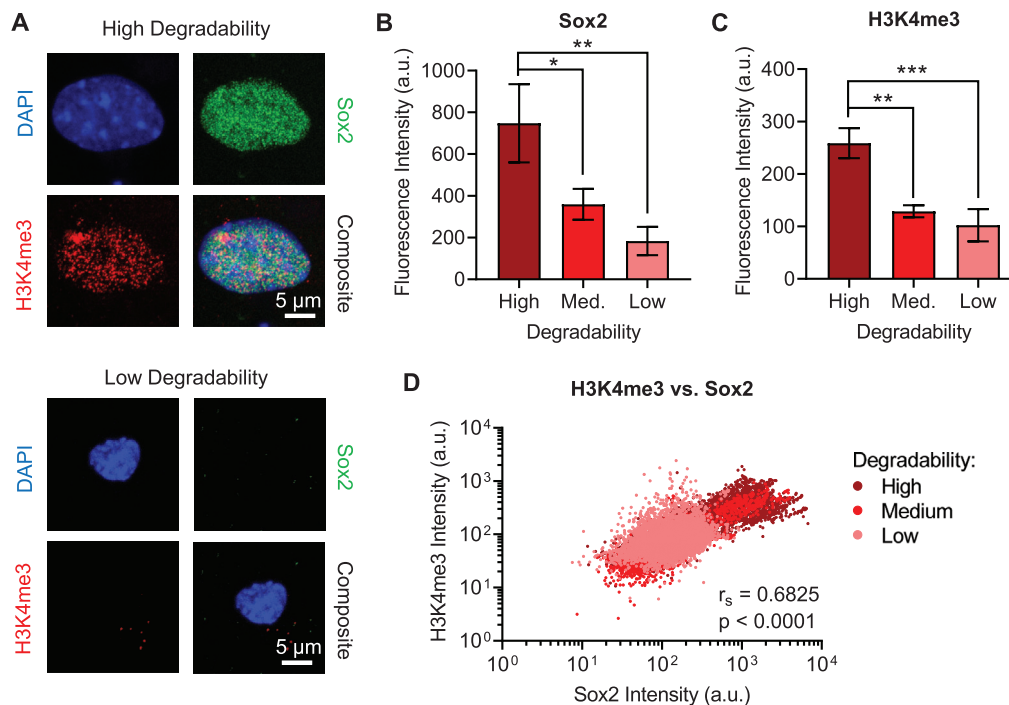


**Figure 3.** High degradability gels and Sox2 positive nuclei are correlated with the activating chromatin mark H3K4me3. A) Representative immunofluorescence images of nuclei from NPCs that were cultured in either high or low degradability hydrogels for 7 days. Blue: DAPI (DNA); green: Sox2; red: H3K4me3. NPCs cultured in high degradability hydrogels exhibit higher B) Sox2 and C) H3K4me3 staining, measured as fluorescence intensity within nuclear (DAPI+) regions of interest (ROIs), compared to NPCs cultured in medium or low degradability gels. Data are presented as mean  $\pm$  s.d.  $n = 3$  independent gels.  $*p < 0.05$ ,  $**p < 0.01$ ,  $***p < 0.001$ , one-way ANOVA with Bonferroni post hoc test. D) Sox2 and H3K4me3 intensity are positively correlated (Spearman correlation) across all three hydrogel degradability conditions tested. Data points represent 8047 nuclear ROIs for high degradability gels, 6119 nuclear ROIs for medium degradability gels, and 6610 nuclear ROIs for low degradability gels. Biaxial plots for H3K4me3 versus Sox2 intensity for individual replicates are presented in Figure S8, Supporting Information.

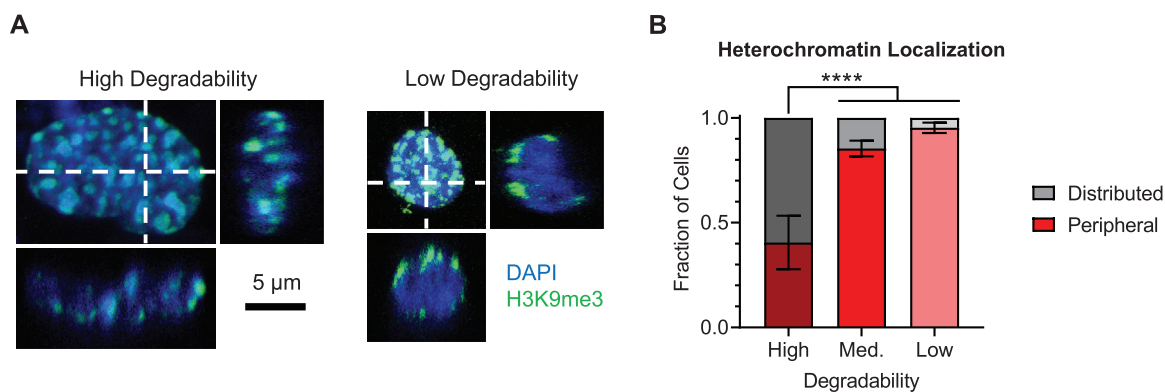


**Figure 4.** Low degradability gels are associated with peripherally localized heterochromatin. A) Representative immunofluorescence images of nuclei from NPCs that were cultured in either high or low degradability hydrogels for 7 days, staining for the heterochromatin mark H3K9me3. Dashed white lines show the imaging planes represented in the XZ and YZ orthogonal views. Blue: DAPI (DNA); green: H3K9me3. B) NPCs cultured in low and medium degradability hydrogels exhibit a greater fraction of cells with peripherally localized heterochromatin, whereas cells in high degradability gels are more likely to have heterochromatin regions distributed throughout the nuclear volume. Data are presented as mean  $\pm$  s.d.  $n = 6$  independent gels.  $****p < 0.0001$ , one-way ANOVA with Bonferroni post hoc test.

marks characteristic of amplifying progenitor cells (Figure 3; Figure S8, Supporting Information). However, the functional phenotype of NPCs in low degradability gels remains unknown. Nearly all cells in low degradability gels have relatively compact nuclei (Figure 1E) and exhibit peripherally localized heterochro-

matin (Figure 4). While proliferative stem cells are known to have some heterochromatin that is dispersed throughout their nuclei, quiescent cells undergo more DNA compaction to silence unnecessary transcription.<sup>[19]</sup> Furthermore, stem cells often silence differentiation-related genes by localizing them within

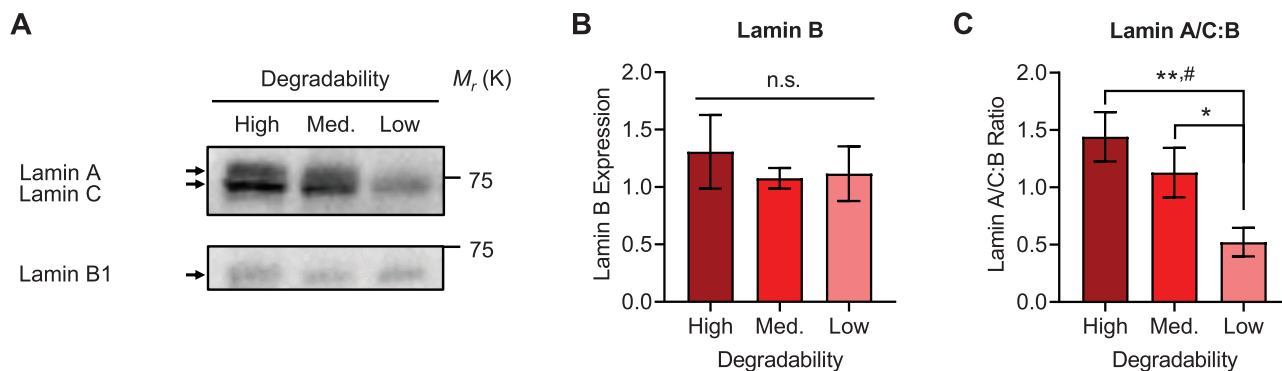


**Figure 5.** Lamin A/C expression varies with hydrogel degradability. A) Representative Western blots for lamin A/C and lamin B1 from NPCs that were cultured in high, medium, or low degradability hydrogels for 7 days. B) Lamin B1 expression does not vary with hydrogel degradability. C) The ratio of lamin A/C:lamin B decreases with decreasing hydrogel degradability. Data are presented as mean  $\pm$  s.d.  $n = 3$  independent gels. \* $p < 0.05$ , \*\* $p < 0.01$ , n.s. = not significant, one-way ANOVA with Bonferroni post hoc test. # $p < 0.05$ , n.s. = not significant, Kruskal–Wallis test with Dunn’s multiple comparisons correction.

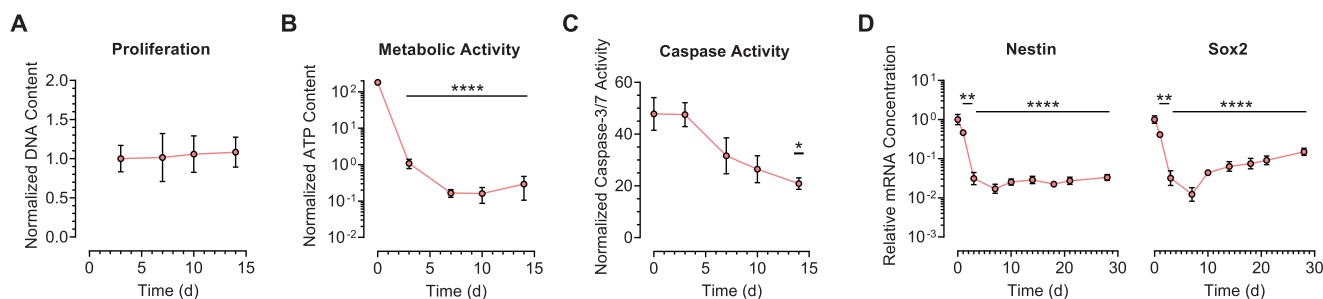


**Figure 6.** NPCs cultured in low degradability gels enter a quiescent-like state but lose expression of stemness markers. A) NPCs cultured in low degradability gels do not exhibit significant proliferation over 14 days in culture, as measured by DNA content. B) The metabolic activity of NPCs cultured in low degradability gels is decreased over 14 days in culture, as measured by ATP content. C) Apoptotic activity remains at or below baseline throughout 14 days of culture in low degradability gels, as measured by caspase-3/7 activity. D) NPCs lose expression of the neural stemness markers nestin and Sox2 during culture in low degradability gels. In (A)–(C), data are presented as mean  $\pm$  s.d. In (A),  $n = 6$ –7 independent gels. In (B),  $n = 5$ –7 independent gels. In (C),  $n = 3$  independent gels. In (D), data are presented as geometric mean with 95% confidence intervals.  $n = 3$ –4 independent gels. \* $p < 0.05$ , \*\* $p < 0.01$ , \*\*\* $p < 0.0001$ , compared to values at day 0, one-way ANOVA with Bonferroni post hoc test.

peripherally localized heterochromatin.<sup>[20]</sup> We therefore postulated that NPCs cultured in low degradability gels might reside in a quiescent state. Consistent with quiescent stem cells, NPCs cultured in low degradability gels do not appreciably proliferate over 14 days in culture (Figure 6A) and significantly decrease their metabolic activity (Figure 6B). Furthermore, NPC apoptotic activity remains at or below baseline over the culture duration, indicating that culture in low degradability gels does not increase cell death (Figure 6C). However, true quiescent stem cells would still be expected to express characteristic stem cell regulators, such as Sox2,<sup>[21]</sup> but NPCs in low degradability gels substantially downregulate expression of nestin and Sox2 (Figure 6D). Thus, NPCs in low degradability gels are not behaving as quiescent neural stem cells in the classical sense.

Nevertheless, we sought to determine if NPCs cultured in low degradability gels maintained the ability to secrete pro-regenerative neurotrophic factors. Enzyme-linked immunosorbent assays (ELISAs) were performed for proteins from two different families of neurotrophins, nerve growth factor (NGF), and ciliary neurotrophic factor (CNTF), after 3 and 7 days of culture in hydrogels with high, medium, or low degradability. Surprisingly, per-cell levels of both NGF and CNTF were significantly higher in

low degradability gels compared to high degradability gels at day 7 (Figure 7A; Figure S10A,B, Supporting Information). Furthermore, the levels of NGF measured in low degradability gels after 7 days in culture was significantly higher than baseline expression of NGF by freshly encapsulated cells (Figure S10C, Supporting Information). To confirm that the neurotrophin secretion was not part of a senescence-associated secretory phenotype (SASP) caused by NPCs becoming senescent in low degradability gels, we performed a time course study of mRNA expression of key senescence genes over 28 days in culture. Across all time points, the senescence markers p16, p21, p53, and p19 are downregulated relative to baseline (Figure 7B). Therefore, the cells cultured in low degradability gels do not appear to be senescent.

To more fully characterize the neurotrophin expression in low degradability gels, the mRNA concentrations of transcripts encoding six neurotrophins, NGF, glial derived neurotrophic factor (GDNF), neurotrophin-3 (NT-3), neurotrophin-4/5 (NT-4/5), brain-derived neurotrophic factor (BDNF), and CNTF, were measured over the course of 28 days in culture (Figure 7C). At the mRNA level, three different trends were observed. Expression of NGF and GDNF did not appreciably change over time, whereas expression of NT-3 and NT-4/5 significantly increased over time.

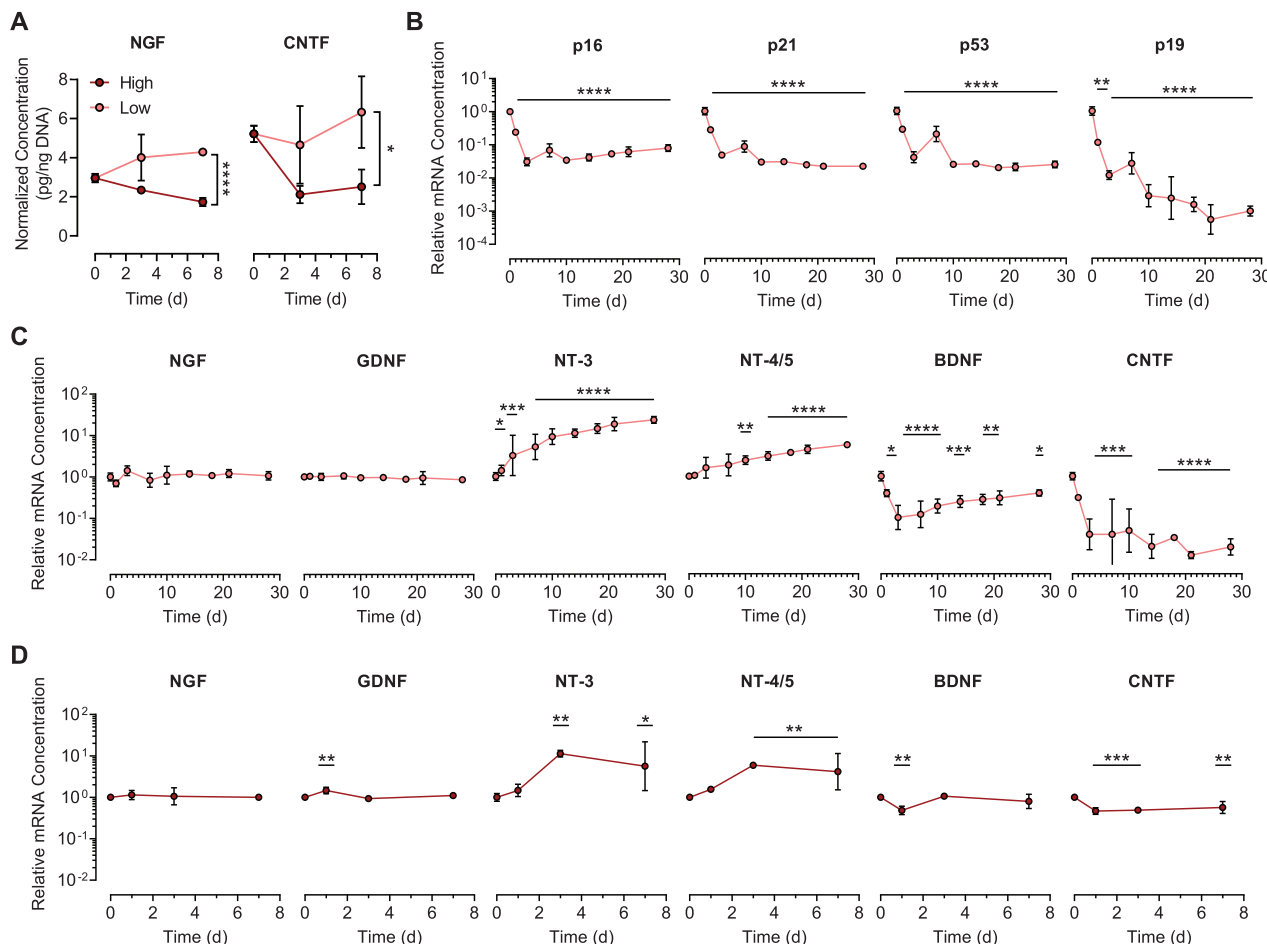


**Figure 7.** NPCs cultured in low degradability hydrogels maintain expression of neurotrophins and downregulate expression of senescence markers. A) NGF and CNTF expression are higher for NPCs cultured in low degradability gels compared to high degradability gels after 7 d in culture. B) mRNA expression for the senescence markers p16, p21, p53, and p19 decreases over 28 days of culture in low degradability gels. C) Quantitative RT-PCR analysis of NPCs cultured in low degradability hydrogels reveals sustained expression of NGF and GDNF, increased expression of NT-3 and NT-4/5, and decreased expression of BDNF and CNTF mRNA over 28 days in culture. D) Expression of neurotrophin mRNAs by NPCs cultured in high degradability gels follows similar trends as NPCs in low degradability gels. In (A), data are presented as mean  $\pm$  s.d.  $n = 3$  independent gels.  $*p < 0.05$ ,  $****p < 0.0001$ , two-tailed Student's  $t$ -test. In (B)–(D), data are presented as geometric mean with 95% confidence intervals.  $n = 3$ –4 independent gels.  $*p < 0.05$ ,  $**p < 0.01$ ,  $***p < 0.001$ ,  $****p < 0.0001$ , compared to mRNA concentration at day 0, one-way ANOVA with Bonferroni post hoc test.

Conversely, expression of BDNF and CNTF decreased over time. Similar trends were observed for NPCs cultured in high degradability gels (Figure 7D). As a whole, these results indicate that NPCs cultured in low degradability gels enter a non-proliferative and low metabolic activity state, but do not senesce, while retaining their neurotrophin secretory phenotype.

### 3. Discussion

#### 3.1. Implications for Materials Applied to NPC Therapies

While numerous preclinical studies have demonstrated positive NPC-mediated effects on nervous system regeneration,<sup>[2,22]</sup> the predominant role played by NPCs is often unclear and may vary based on the therapeutic target.<sup>[23]</sup> In some instances, NPCs are believed to aid in regeneration by differentiating into mature cell types such as neurons and oligodendrocytes and directly re-

placing damaged or diseased tissue.<sup>[2]</sup> Such outcomes would be highly desirable for conditions characterized by significant death of a particular neuronal cell type, as occurs in many neurodegenerative diseases. On the other hand, NPCs are also known to secrete neurotrophic factors that modulate the host cell response to injury, and this paracrine effect can drive tissue regeneration without relying on the differentiation and integration of transplanted NPCs into the host tissue.<sup>[3]</sup> This role for NPCs may be useful for traumatic injuries such as spinal cord injury, wherein transplanted NPCs could guide damaged axons to reconnect with their targets and reduce scarring through paracrine effects.

Based on the results of the present study and our previously published work,<sup>[9,10]</sup> materials designed to deliver NPCs for tissue replacement therapies should enable significant NPC-mediated remodeling to best maintain NPC stemness. NPCs cultured in high degradability gels express high levels of the neural stemness markers nestin and Sox2 (Figure 1B,C; Figure S3, Supporting Information), indicating that

the cells maintain their multipotent differentiation potential. Consistent with this finding, our previously published studies demonstrated enhanced differentiation potential and neuronal maturation for NPCs cultured in high degradability gels.<sup>[9,10]</sup> Furthermore, NPCs cultured in high degradability gels exhibited higher proliferative capacity (Figure 1B,D) and increased levels of activating epigenetic marks (Figure 3) characteristic of amplifying progenitor cells,<sup>[13]</sup> suggesting that NPCs in highly remodelable materials are capable of generating a large number of progeny to participate in tissue regeneration.

In contrast, for applications where transplanted NPCs are intended predominantly for trophic support, less remodelable materials may be desirable. NPCs in low degradability gels maintain expression of neurotrophins such as NGF and GDNF over the course of 28 days in culture and upregulate expression of others, including NT-3 and NT-4/5 (Figure 7C). Previous approaches have engineered NPCs to overexpress neurotrophins to aid in neural regeneration.<sup>[24]</sup> The observation that 3D encapsulation within low degradability gels can trigger endogenous pathways to upregulate NT-3 and NT-4/5 suggests a promising alternative approach that avoids genetic modification of the cells. Furthermore, NPCs encapsulated in low degradability gels do not appreciably proliferate (Figure 1B,D; Figure 6A), mitigating the risk of tumor formation from highly proliferative cells. Finally, NPCs in low degradability gels do not express classical senescence markers (Figure 7B), and we have previously shown that they do not spontaneously differentiate into neurons, astrocytes, or oligodendrocytes,<sup>[10]</sup> limiting the potential off-target effects of cell transplantation. Future studies in animal models will be needed to confirm that encapsulated NPCs maintain a similar secretory profile in vivo to determine if this potential therapeutic approach is worth pursuing.

### 3.2. Regulation of Nuclear Organization by Matrix Degradability

This study reports a previously unrecognized role of matrix degradability in regulating nuclear organization in encapsulated NPCs. Nuclei of NPCs in high degradability gels are significantly larger and less round than nuclei of NPCs in low degradability gels, with the large, elongated nuclear morphology correlated with Sox2 expression and EdU incorporation (Figure 1D; Figure 2; Figures S4–S7, Supporting Information). We have previously shown that increasing hydrogel degradability facilitates increased cell spreading.<sup>[9]</sup> Increased spreading could apply more tension on the nucleus, encouraging nuclear elongation. Increased lamin A/C expression has been shown to increase nuclear stiffness, which in turn enhances nuclear mechanical integrity.<sup>[18,25]</sup> Lamin A/C deficiency results in poor nuclear stability, leading to nuclear rupture and DNA damage.<sup>[26]</sup> Thus, we speculate that the higher levels of lamin A/C observed in high degradability gels serve to better stabilize nuclei under tension in spread cells. NPCs in low degradability gels do not appreciably spread,<sup>[9]</sup> reducing the stress on the nuclei, consistent with a decrease in the ratio of A-type to B-type lamins (Figure 5C).

We have previously demonstrated that hydrogel degradability regulates  $\beta$ -catenin activity, and that active  $\beta$ -catenin signaling is necessary for expression of stemness factors in encapsulated NPCs.<sup>[9]</sup> In our prior work, N-cadherin cell–cell contacts that are

maintained through matrix remodeling upregulate  $\beta$ -catenin signaling, driving expression of the transcriptional co-activator Yes-associated protein (YAP), enabling stemness maintenance and subsequent differentiation.<sup>[9,10]</sup> Interestingly, decreased lamin A/C levels have been correlated with decreased signaling via the  $\beta$ -catenin pathway,<sup>[27]</sup> and here we demonstrate that low degradability gels, which are known to have decreased  $\beta$ -catenin signaling,<sup>[9]</sup> also have decreased expression of lamin A/C. This suggests that altered nuclear lamina composition may feedback on other biochemical mechanisms regulating cell state to modulate NPC stemness.

### 3.3. Future Directions

Our results indicate a correlation between matrix degradation and NPC epigenetics and secretome that may have significant therapeutic implications for neural precursors. This work has highlighted new questions that should be addressed to characterize NPC-material interactions, both in terms of basic biology and clinical applicability. Further work is necessary to determine if changes in nuclear lamina composition are biochemically regulated by changes in matrix degradability and if the altered lamina is in turn responsible for epigenetic regulation. For instance, B-type lamins are known to bind to heterochromatin through the lamin-associated proteins LBR and HP1, with HP1 interacting with the inactivating H3K9me3 histone mark.<sup>[15]</sup> B-type lamin-mediated tethering of heterochromatin has been shown to maintain an undifferentiated state in myogenic cells,<sup>[28]</sup> providing a potential mechanism whereby low matrix degradability can induce a quiescence-like (i.e., non-proliferative and low metabolic activity) state in NPCs by sequestering heterochromatin to the nuclear periphery. Such changes in chromatin localization regulating gene silencing could explain why activated NPCs in high degradability gels have more distributed chromatin, namely to permit increased access to stemness and differentiation-related genes. Further, incorporation of lamin A and lamin C isoforms into the nuclear lamina has been shown to be regulated by distinct biochemical mechanisms,<sup>[29]</sup> suggesting that the apparent difference we observed in lamin A versus C expression may also play a role in epigenetic regulation and nuclear mechanics.<sup>[30]</sup>

For future clinical applications, several outstanding questions remain before differences in engineered ECM degradability can be considered as a mechanism for regulating therapeutic delivery of neurotrophins. The choice of material employed will be a significant consideration not just from a biocompatibility standpoint, but also for how the material may interact with neurotrophins secreted by encapsulated NPCs. ELPs are an attractive material for this application, as altering matrix degradability does not alter the microstructure of the materials,<sup>[9]</sup> and thus does not alter the diffusion of macromolecules of comparable size to the neurotrophins studied (Figure S11, Supporting Information). However, neurotrophins can still be sequestered within materials by interactions with cell-secreted ECM. Matrix remodeling consists of both degradation of existing matrix and production of new matrix,<sup>[31]</sup> and NPCs are known to produce ECM in 3D cultures.<sup>[32]</sup> Thus, future work should assess fouling of the engineered materials by cell-secreted ECM to ensure secreted neurotrophins are not trapped within the hydrogels. Ultimately, the



availability and bioactivity of secreted neurotrophins that are released from the hydrogels will dictate the therapeutic relevance of this strategy. As such, future experiments will need to assess the concentration and activity of neurotrophins of interest from the cell culture supernatants of NPCs cultured in low degradability gels before proceeding with *in vivo* studies investigating regenerative potential. Finally, the present study is limited to murine NPCs, whereas clinical applications will require human-derived NPCs. Studies assessing the impact of matrix degradation on human stem cell-derived NPCs are ongoing.

## 4. Conclusion

Matrix remodelability influences the chromatin organization and neurotrophin expression of encapsulated NPCs. High degradability gels promote maintenance of an activated stem cell phenotype characterized by elevated Sox2 expression and EdU incorporation. NPC nuclear morphology varies with hydrogel degradability, as NPCs in high degradability gels have larger, more oblong nuclei than NPCs in low degradability gels. Nuclear morphology is tightly correlated with stemness, as Sox2+ and EdU+ nuclei are larger and less round than Sox2- and EdU- nuclei across all degradability conditions. Further, changes in nuclear morphology are associated with altered chromatin states, as large Sox2+ nuclei co-stain for higher levels of the activating histone mark H3K4me3, while small, rounded nuclei exhibit peripherally localized heterochromatin. These differences in nuclear morphology and chromatin organization occur along with altered lamin expression, as NPCs in high degradability hydrogels express higher levels of lamin A/C than NPCs in low degradability gels. In contrast, NPCs in low degradability gels express higher levels of NGF than cells in high degradability gels. In low degradability gels, NPCs enter a non-proliferative, low metabolic activity state that is not characterized by classical senescence markers, while still expressing multiple neurotrophins. These results suggest that NPCs cultured in high degradability gels may be best suited to applications involving stem cell expansion for tissue replacement therapies, while NPCs embedded in low degradability gels may be useful to guide neural regeneration through secretion of paracrine factors.

## 5. Experimental Section

**Materials:** All materials were purchased from either Sigma-Aldrich or Fisher Scientific and used as received, unless otherwise noted.

**ELP Hydrogel Production:** Recombinant ELPs containing an extended RGD amino acid sequence derived from human fibronectin and an ADAM9 proteolysis site were produced as described in detail elsewhere.<sup>[9,10,33]</sup> Briefly, the gene encoding the ELP was cloned into a pET-15b plasmid and transformed into BL21(DE3)pLysS *Escherichia coli*. Bacteria were grown in Terrific Broth until an optical density of 0.8, and ELP expression was induced with isopropyl  $\beta$ -D-1-thiogalactopyranoside (IPTG). The bacteria were collected by centrifugation and lysed by repetitive freeze-thaw cycles. The ELP was purified by inverse thermal cycling, dialyzed against MilliQ-grade water, and lyophilized to afford a white, fluffy solid. Protein purity was confirmed by sodium dodecylsulfate-polyacrylamide gel electrophoresis (SDS-PAGE).

To prepare hydrogels, ELP was dissolved overnight at 4 °C in Dulbecco's phosphate buffered saline (PBS) to 3.75% w/v and sterile filtered

(0.22  $\mu$ m). Separately, stock solutions of THPC were prepared in PBS, such that the final concentration of THPC afforded a stoichiometric ratio of 0.5:1 (high degradability), 0.75:1 (medium degradability), or 1:1 (low degradability) THPC hydroxymethyls to lysine primary amines when mixed in a 1:4 volumetric ratio with the ELP solution (to yield a final ELP concentration of 3% w/v). ELP hydrogels were prepared by mixing ELP and THPC solutions on ice and transferring the pre-gel solution to custom cylindrical silicone molds (0.5 mm high  $\times$  2–5 mm diameter). The crosslinking reaction was allowed to proceed at room temperature for 15 min, followed by 15 min at 37 °C. Hydrogel elastic moduli in unconfined compression were determined using an ARG2 rheometer, as previously described.<sup>[9]</sup> Hydrogel degradability was measured following our previously published protocol using Cy5-labeled ELP to track bulk material erosion from hydrogels with encapsulated NPCs.<sup>[9,10]</sup> Macromolecular diffusivity within the hydrogels was measured by fluorescence recovery after photobleaching (FRAP) of fluorescein isothiocyanate (FITC)-labeled dextrans (Sigma), as previously described.<sup>[9]</sup>

**NPC Culture and Encapsulation:** Murine hippocampal NPCs isolated from microdissected dentate gyrus were kindly provided by Prof. Theo Palmer (Stanford Neurosurgery).<sup>[34]</sup> NPCs were maintained on polyornithine and laminin-coated tissue culture plastic in Neurobasal-A medium supplemented with 2% B27, 1% GlutaMAX (Gibco), 20 ng mL<sup>-1</sup> FGF-2, and 20 ng mL<sup>-1</sup> EGF (PeproTech). Prior to encapsulation in ELP hydrogels, NPCs were lifted by trypsinization, washed, and counted. NPCs were pelleted by centrifugation and resuspended in a 3.75% w/v ELP solution in PBS such that the final NPC concentration was  $5 \times 10^7$  cells mL<sup>-1</sup>. Hydrogels were prepared by mixing with the desired concentration of THPC as described above to yield hydrogels with high, medium, or low degradability. The NPC-containing hydrogels were covered with maintenance medium and cultured in a 37 °C, 5% CO<sub>2</sub> incubator.

**Immunofluorescence Analysis:** Immunofluorescence staining of NPCs encapsulated within ELP hydrogels was performed according to our previously published protocols.<sup>[9,10,33]</sup> Samples were fixed in 4% paraformaldehyde in PBS at 37 °C for 30 min and washed with PBS. Cells were permeabilized with PBS plus Triton X-100 (PBST), blocked with bovine serum albumin and goat serum, and incubated with primary antibodies (see Table S1, Supporting Information) overnight at 4 °C. The samples were then extensively washed with PBST at room temperature before being incubated with secondary antibodies (goat anti-mouse AF647, 1:500; goat anti-rabbit AF488, 1:500; goat anti-rabbit AF546, 1:500; Life Technologies) and 4',6-diamidino-2-phenylindole dihydrochloride (DAPI) overnight at 4 °C. Samples were again washed with PBST and mounted on glass coverslips using Vectashield hardset mounting medium (Vector Laboratories). For EdU staining, cells were treated with medium containing F-ara-EdU (10  $\mu$ M)<sup>[35]</sup> for 24 h prior to fixation. Prior to blocking, samples were then treated with 10  $\mu$ M AF488-azide (Life Technologies) in 100 mM Tris, 1 mM copper(II) chloride, and 100 mM ascorbic acid, pH 8.5 for 1 h at room temperature to label incorporated EdU.<sup>[36]</sup> Samples were imaged on a Leica SPE confocal microscope.

Image analysis was performed using ImageJ (NIH). For the nuclear morphology and Sox2/EdU positivity analysis presented in Figures 1 and 2, confocal Z-stacks were separated into 3–5 Z-position sub-stacks and max-projected to obtain 2D images. The nuclei were identified by generating binary masks based on the DAPI channel, and these masks were used to define ROIs. Consecutive projections were compared to ensure that nuclei were not double counted. Nuclear morphology (projected area and roundness) was analyzed using the Analyze Particles function. Sox2 and EdU positivity were determined by selecting a fixed fluorescence intensity threshold and applying this threshold across all data sets. For the H3K4me3/Sox2 correlation analysis presented in Figure 3, binary Z-stacks were generated from the DAPI channel to selectively measure Sox2 and H3K4me3 staining intensity within nuclear ROIs. These nuclear ROIs were overlaid with the Sox2 and H3K4me3 channels, and the fluorescence intensity within the ROIs was measured. The same ROIs were used across both channels to enable correlation analysis between the Sox2 and H3K4me3 signals.

**Western Blot Analysis:** Western blots to measure lamin expression were performed according to our published protocols.<sup>[9,10]</sup> Briefly,

hydrogels containing NPCs were removed from their silicone molds and transferred to a microcentrifuge tube containing cold radioimmunoprecipitation assay (RIPA) buffer (Cell Signaling Technology) with protease and phosphatase inhibitors (Roche). The hydrogels were mechanically disrupted by sonication, and the lysates were clarified by centrifugation. The supernatants were collected, and protein content was quantified (Bio-Rad DC Protein Assay). 25 µg of protein per sample were separated by SDS-PAGE and transferred to a polyvinylidene difluoride membrane. The membrane was blocked with non-fat milk (NFM) in Tris-buffered saline with Tween-20 (TBST) at room temperature for 1 h and then incubated with primary antibodies (see Table S1, Supporting Information) diluted in NFM in TBST overnight at 4 °C. The blots were washed with TBST, incubated with horseradish peroxidase-conjugated secondary antibodies (donkey anti-mouse, 1:10 000; donkey anti-rabbit, 1:10 000; Jackson ImmunoResearch) in TBST for 1 h at room temperature. The blots were washed with TBST, developed using West Pico or Femto Chemiluminescent Substrates (Pierce), and imaged using a ChemiDoc MP gel imaging system (Bio-Rad). Quantitative densitometry was performed using ImageJ, and the intensity of each band was normalized to the background intensity of the respective lane to account for differences in exposure levels across the blots.

**Gene Expression Analysis:** Gene expression was measured by quantitative reverse transcription-polymerase chain reaction (qRT-PCR) following our established protocols.<sup>[9,10]</sup> Briefly, NPC-containing hydrogels were transferred to TRIzol reagent (Life Technologies) and mechanically disrupted by sonication. RNA was purified by phenol-chloroform extraction using phase-lock gels (5 Prime). 1 µg of RNA was reverse transcribed (Applied Biosystems High-Capacity cDNA Reverse Transcription Kit), and the concentration of the resulting cDNA was adjusted to achieve consistent loading across samples. PCR was performed using Fast SYBR Green Master Mix (Applied Biosystems) on an Applied Biosystems StepOnePlus Real Time PCR System. Primers are listed in Table S2, Supporting Information.

**Biochemical Analyses:** For DNA content, ATP content, caspase-3/7 activity, and ELISAs, gels were transferred to lysis buffer (20 mM Tris HCl, 150 mM NaCl, 0.5% Triton X-100, pH 7.4) and mechanically disrupted by sonication. Lysates were used without further processing for DNA, ATP, and caspase assays. DNA content was measured using the Quant-iT PicoGreen dsDNA Assay Kit (Life Technologies), following the manufacturer's instructions. ATP content was measured using the CellTiter Glo Luminescent Cell Viability Assay (Promega) and relating lysate luminescence to ATP content based on a standard curve. Caspase-3/7 activity was measured using the Apo-ONE Homogeneous Caspase-3/7 Assay (Promega) and relating lysate fluorescence to caspase activity based on a standard curve generated using recombinant human caspase-3 (Millipore). ATP content and caspase activity were normalized to DNA content. For ELISAs, whole gel lysates were used in order to capture all possible locations of produced neurotrophins: intracellular, hydrogel associated, and soluble. Lysates were first clarified by centrifugation to pellet insoluble material and DNA. The supernatants were used to measure NGF and CNTF concentration using the Human  $\beta$ -NGF Mini ABTS ELISA Development Kit and the Rat CNTF Mini ABTS ELISA Development Kit (PeproTech), following the manufacturer's instructions. DNA content in the centrifuged pellets was measured using the Quant-iT PicoGreen dsDNA Assay Kit as above after resuspending the pellets in Tris-EDTA (TE) buffer. NGF and CNTF concentrations were normalized to DNA content.

**Statistical Analysis:** All statistical analyses were performed using GraphPad Prism 8. Comparisons among more than two experimental groups or time points were performed using one-way analysis of variance (ANOVA) with Bonferroni post hoc testing. Due to a low  $n$ , comparison of lamin A/C expression also used a nonparametric Kruskal–Wallis test with Dunn's multiple comparison correction that does not assume a normal distribution. Comparisons of nuclear area and roundness distributions were performed using a Kolmogorov–Smirnov test. Correlation testing between Sox2 and H3K4me3 levels was performed using a nonparametric Spearman correlation test. Comparisons of nuclear morphology parameters within a given hydrogel degradability and comparisons of NGF and CNTF expression relative to baseline were performed using two-tailed Student's  $t$ -tests with Holm–Sidak multiple comparisons corrections.

$p$ -values of less than 0.05 were considered statistically significant. For analysis of qRT-PCR data, statistical analysis was performed prior to transforming to a natural scale.<sup>[37]</sup> Relative mRNA expression was reported as a geometric mean with asymmetric 95% confidence intervals derived from the logarithmic scale data.

## Supporting Information

Supporting Information is available from the Wiley Online Library or from the author.

## Acknowledgements

The authors would like to thank Prof. Theo Palmer and Dr. Harish Babu (Stanford Neurosurgery) for providing the adult murine neural progenitor cells. C.M.M. was supported by a Ruth L. Kirschstein NRSA F31 fellowship (F31 EB020502) from the National Institutes of Health (NIH), the Siebel Scholars Program, and the Open Philanthropy Project through a Life Sciences Research Foundation (LSRF) postdoctoral fellowship. B.L.L. was supported by the Stanford University Bio-X Bowes Graduate Fellowship. This work was supported by funding from the National Institutes of Health (R01 HL142718, R01 EB027171, R01 EB027666).

## Conflict of Interest

The authors declare no conflict of interest.

## Keywords

chromatin organization, elastin-like proteins, hydrogels, matrix degradation, neural stem/progenitor cells

Received: May 4, 2020

Revised: July 14, 2020

Published online:

- [1] S. Goldman, *Nat. Biotechnol.* **2005**, *23*, 862.
- [2] S. Wu, K. T. FitzGerald, J. Giordano, *Front. Neurol.* **2018**, *9*, 602.
- [3] C. M. Willis, A. M. Nicaise, L. Peruzzotti-Jametti, S. Pluchino, *Brain Res.* **2020**, *1729*, 146615.
- [4] S. Irion, S. E. Zabierowski, M. J. Tomishima, *Mol. Ther.–Methods Clin. Dev.* **2017**, *4*, 72.
- [5] K. G. Chen, B. S. Mallon, R. D. G. McKay, P. G. Robey, *Cell Stem Cell* **2014**, *14*, 13.
- [6] C. M. Madl, S. C. Heilshorn, H. M. Blau, *Nature* **2018**, *557*, 335.
- [7] a) M. W. Tibbitt, K. S. Anseth, *Biotechnol. Bioeng.* **2009**, *103*, 655; b) S. R. Caliani, J. A. Burdick, *Nat. Meth.* **2016**, *13*, 405.
- [8] a) X. Li, E. Katsanevakis, X. Liu, N. Zhang, X. Wen, *Prog. Polym. Sci.* **2012**, *37*, 1105; b) P. Madhusudanan, G. Raju, S. Shankarappa, *J. R. Soc., Interface* **2020**, *17*, 20190505.
- [9] C. M. Madl, B. L. LeSavage, R. E. Dewi, C. B. Dinh, R. S. Stowers, M. Khariton, K. J. Lampe, D. Nguyen, O. Chaudhuri, A. Enejder, S. C. Heilshorn, *Nat. Mater.* **2017**, *16*, 1233.
- [10] C. M. Madl, B. L. LeSavage, R. E. Dewi, K. J. Lampe, S. C. Heilshorn, *Adv. Sci.* **2019**, *6*, 1801716.
- [11] K. S. Straley, S. C. Heilshorn, *Soft Matter* **2009**, *5*, 114.
- [12] a) H. Santos-Rosa, R. Schneider, A. J. Bannister, J. Sherriff, B. E. Bernstein, N. C. T. Emre, S. L. Schreiber, J. Mellor, T. Kouzarides, *Nature* **2002**, *419*, 407; b) R. Schneider, A. J. Bannister, F. A. Myers, A. W. Thorne, C. Crane-Robinson, T. Kouzarides, *Nat. Cell Biol.* **2004**, *6*, 73.

- [13] R. S. Sandstrom, M. R. Foret, D. A. Grow, E. Haugen, C. T. Rhodes, A. E. Cardona, C. F. Phelix, Y. Wang, M. S. Berger, C.-H. A. Lin, *Sci. Rep.* **2015**, *4*, 5371.
- [14] R. C. Allshire, H. D. Madhani, *Nat. Rev. Mol. Cell Biol.* **2018**, *19*, 229.
- [15] Y. Gruenbaum, R. Foisner, *Annu. Rev. Biochem.* **2015**, *84*, 131.
- [16] K. N. Dahl, A. J. S. Ribeiro, J. Lammerding, *Circ. Res.* **2008**, *102*, 1307.
- [17] R. D. Goldman, Y. Gruenbaum, R. D. Moir, D. K. Shumaker, T. P. Spann, *Genes Dev.* **2002**, *16*, 533.
- [18] J. Swift, I. L. Ivanovska, A. Buxboim, T. Harada, P. C. D. P. Dingal, J. Pinter, J. D. Pajeroski, K. R. Spinler, J.-W. Shin, M. Tewari, F. Rehfeldt, D. W. Speicher, D. E. Discher, *Science* **2013**, *341*, 1240104.
- [19] S. Srivastava, R. K. Mishra, J. Dhawan, *Organogenesis* **2010**, *6*, 37.
- [20] a) R. R. E. Williams, V. Azuara, P. Perry, S. Sauer, M. Dvorkina, H. Jørgensen, J. Roix, P. McQueen, T. Misteli, M. Merkenschlager, A. G. Fisher, *J. Cell Sci.* **2006**, *119*, 132; b) V. Boonsanay, T. Zhang, A. Georgieva, S. Kostin, H. Qi, X. Yuan, Y. Zhou, T. Braun, *Cell Stem Cell* **2016**, *18*, 229.
- [21] a) H. Suh, A. Consiglio, J. Ray, T. Sawai, K. A. D'Amour, F. H. Gage, *Cell Stem Cell* **2007**, *1*, 515; b) S. Lugert, O. Basak, P. Knuckles, U. Haussler, K. Fabel, M. Götz, C. A. Haas, G. Kempermann, V. Taylor, C. Giachino, *Cell Stem Cell* **2010**, *6*, 445.
- [22] W. Tetzlaff, E. B. Okon, S. Karimi-Abdolrezaee, C. E. Hill, J. S. Sparling, J. R. Plemel, W. T. Plunet, E. C. Tsai, D. Baptiste, L. J. Smithson, M. D. Kawaja, M. G. Fehlings, B. K. Kwon, *J. Neurotrauma* **2011**, *28*, 1611.
- [23] G. Martino, S. Pluchino, *Nat. Rev. Neurosci.* **2006**, *7*, 395.
- [24] a) P. Lu, L. L. Jones, E. Y. Snyder, M. H. Tuszynska, *Experim. Neurol.* **2003**, *181*, 115; b) H. J. Lee, I. J. Lim, M. C. Lee, S. U. Kim, *J. Neurosci. Res.* **2010**, *88*, 3282; c) J. Butenschön, T. Zimmermann, N. Schmarowski, R. Nitsch, B. Fackelmeier, K. Friedemann, K. Radyushkin, J. Baumgart, B. Lutz, J. Leschik, *Stem Cell Res. Ther.* **2016**, *7*, 11; d) H. J. Lee, I. H. Park, H. J. Kim, S. U. Kim, *Gene Ther.* **2009**, *16*, 1066; e) H. E. S. Marei, A. Farag, A. Althani, N. Affi, A. Abd-Elmaksoud, S. Lashen, S. Rezk, R. Pallini, P. Casalbore, C. Cenciarelli, *J. Cell. Physiol.* **2015**, *230*, 116.
- [25] J. Lammerding, L. G. Fong, J. Y. Ji, K. Reue, C. L. Stewart, S. G. Young, R. T. Lee, *J. Biol. Chem.* **2006**, *281*, 25768.
- [26] a) T. Sullivan, D. Escalante-Alcalde, H. Bhatt, M. Anver, N. Bhat, K. Nagashima, C. L. Stewart, B. Burke, *J. Cell Biol.* **1999**, *147*, 913; b) J. Lammerding, P. C. Schulze, T. Takahashi, S. Kozlov, T. Sullivan, R. D. Kamm, C. L. Stewart, R. T. Lee, *J. Clin. Invest.* **2004**, *113*, 370; c) W. H. De Vos, F. Houben, M. Kamps, A. Malhas, F. Verheyen, J. Cox, E. M. M. Manders, V. L. R. M. Verstraeten, M. A. M. van Steensel, C. L. M. Marcelis, A. van den Wijngaard, D. J. Vaux, F. C. S. Ramaekers, J. L. V. Broers, *Hum. Mol. Genet.* **2011**, *20*, 4175; d) N. Y. Chen, P. Kim, T. A. Weston, L. Edillo, Y. Tu, L. G. Fong, S. G. Young, *Proc. Natl. Acad. Sci. USA* **2018**, *115*, 10100.
- [27] a) V. Andrés, J. M. González, *J. Cell Biol.* **2009**, *187*, 945; b) S. Bermeo, C. Vidal, H. Zhou, G. Duque, *J. Cell. Biochem.* **2015**, *116*, 2344; c) C. Le Dour, C. Macquart, F. Sera, S. Homma, G. Bonne, J. P. Morrow, H. J. Worman, A. Muchir, *Hum. Mol. Genet.* **2017**, *26*, 333.
- [28] I. Solovei, A. S. Wang, K. Thanisch, C. S. Schmidt, S. Krebs, M. Zwirger, T. V. Cohen, D. Devys, R. Foisner, L. Peichl, H. Herrmann, H. Blum, D. Engelkamp, C. L. Stewart, H. Leonhardt, B. Joffe, *Cell* **2013**, *152*, 584.
- [29] G. E. Pugh, P. J. Coates, E. B. Lane, Y. Raymond, R. A. Quinlan, *J. Cell Sci.* **1997**, *110*, 2483.
- [30] R. D. González-Cruz, K. N. Dahl, E. M. Darling, *Front. Cell Dev. Biol.* **2018**, *6*, 151.
- [31] U. Blache, M. M. Stevens, E. Gentleman, *Nat. Biomed. Eng.* **2020**, *4*, 357.
- [32] D. Simão, M. M. Silva, A. P. Terrasso, F. Arez, M. F. Q. Sousa, N. Z. Mehrjardi, T. Šarić, P. Gomes-Alves, N. Raimundo, P. M. Alves, C. Brito, *Stem Cell Rep.* **2018**, *11*, 552.
- [33] B. L. LeSavage, N. A. Suhar, C. M. Madl, S. C. Heilshorn, *J. Visualized Exp.*, e57739. <http://doi.org/10.3791/57739>.
- [34] H. Babu, G. Cheung, H. Kettenmann, T. D. Palmer, G. Kempermann, *PLoS One* **2007**, *2*, e388.
- [35] A. B. Neef, N. W. Luedtke, *Proc. Natl. Acad. Sci. USA* **2011**, *108*, 20404.
- [36] A. Salic, T. J. Mitchison, *Proc. Natl. Acad. Sci. USA* **2008**, *105*, 2415.
- [37] N. H. Romano, C. M. Madl, S. C. Heilshorn, *Acta Biomater.* **2015**, *11*, 48.